Thermal resistance and heat capacity in hafnium zirconium oxide ($Hf_{1-x}Zr_xO_2$) dielectrics and ferroelectric thin films

Ethan A. Scott, Sean W. Smith, M. David Henry, Christina M. Rost, Ashutosh Giri, John T. Gaskins, Shelby S. Fields, Samantha T. Jaszewski, Jon F. Ihlefeld, and Patrick E. Hopkins

Citation: Appl. Phys. Lett. **113**, 192901 (2018); doi: 10.1063/1.5052244
View online: https://doi.org/10.1063/1.5052244
View Table of Contents: http://aip.scitation.org/toc/apl/113/19
Published by the American Institute of Physics

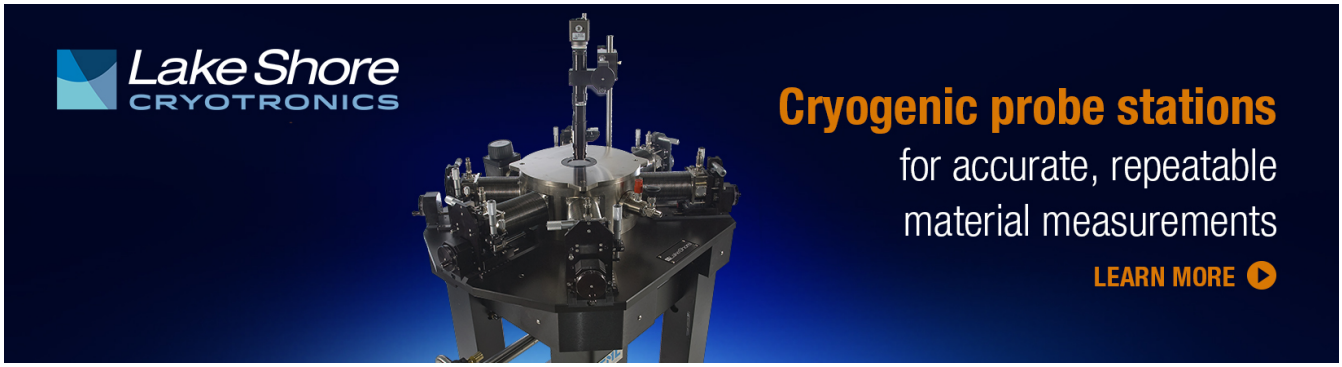

Reuse of AIP Publishing content is subject to the terms at: https://publishing.aip.org/authors/rights-and-permissions. Downloaded to: 63.88.101.67 on 07 November 2018, At: 12:27

Thermal resistance and heat capacity in hafnium zirconium oxide ($Hf_{1-x}Zr_xO_2$) dielectrics and ferroelectric thin films

Ethan A. Scott,[1] Sean W. Smith,[2] M. David Henry,[2] Christina M. Rost,[1] Ashutosh Giri,[1] John T. Gaskins,[1] Shelby S. Fields,[3] Samantha T. Jaszewski,[3] Jon F. Ihlefeld,[3,4] and Patrick E. Hopkins[1,3,5,a)]

[1]*Department of Mechanical and Aerospace Engineering, University of Virginia, Charlottesville, Virginia 22904, USA*
[2]*Sandia National Laboratories, Albuquerque, New Mexico 87185, USA*
[3]*Department of Materials Science and Engineering, University of Virginia, Charlottesville, Virginia 22904, USA*
[4]*Department of Electrical and Computer Engineering, University of Virginia, Charlottesville, Virginia 22904, USA*
[5]*Department of Physics, University of Virginia, Charlottesville, Virginia 22904, USA*

(Received 15 August 2018; accepted 23 October 2018; published online 7 November 2018)

We report on the thermal resistances of thin films (20 nm) of hafnium zirconium oxide ($Hf_{1-x}Zr_xO_2$) with compositions ranging from $0 \leq x \leq 1$. Measurements were made via time-domain thermoreflectance and analyzed to determine the effective thermal resistance of the films in addition to their associated thermal boundary resistances. We find effective thermal resistances ranging from 28.79 to 24.72 $m^2\,K\,GW^{-1}$ for amorphous films, which decreased to 15.81 $m^2\,K\,GW^{-1}$ upon crystallization. Furthermore, we analyze the heat capacity for two compositions, $x = 0.5$ and $x = 0.7$, of $Hf_{1-x}Zr_xO_2$ and find them to be 2.18 ± 0.56 and $2.64 \pm 0.53\,MJ\,m^{-3}\,K^{-1}$, respectively. *Published by AIP Publishing.* https://doi.org/10.1063/1.5052244

Due to their unique ferroelectric behavior, ease of manufacture, and inherent silicon compatibility, HfO_2-based systems have recently begun to garner attention as potential candidates for non-volatile memory, negative differential capacitance transistors, and energy harvesting applications, among others.[1–4] Since ferroelectric properties were first demonstrated in 2011,[5] various factors have been shown to allow stability of the ferroelectric phase, including alloying with Zr,[6] depositing onto a nitride electrode layer such as TaN,[7] as well as tuning the grain size and film thickness.[6,8,9] The ferroelectric response of HfO_2-based films is attributed to the polar crystalline structure inherent to the orthorhombic $Pca2_1$ phase.[1,7] When alloyed with ZrO_2, ferroelectricity in $Hf_{1-x}Zr_xO_2$ systems can be tuned with a field-induced phase transition from the tetragonal to orthorhombic phase,[10] which broadens the horizons for application in energy storage devices as well as electronic memory devices and architectures.[1]

While ample studies have focused upon the electrical and structural properties of $Hf_{1-x}Zr_xO_2$ systems,[1,5–11] there exists a gap in the literature in terms of their thermal properties, particularly in thin-film form. Even for pure hafnia or zirconia, the literature on thermal properties is limited, especially with regard to heat capacity.[12] The preferred method of fabrication for $Hf_{1-x}Zr_xO_2$ films is atomic layer deposition (ALD),[1,11] and though prior studies have reported measurements of the thermal conductivity of ALD grown HfO_2[13–16] films, there have been no studies investigating their thermal properties when alloyed with ZrO_2. Furthermore, given the potential for HfO_2-based materials to impact infrared sensing and thermal energy harvesting applications, knowledge of the thermal properties is vital to CMOS integrated device development.[17]

In this study, we measure the thermal resistance and effective thermal conductivity of $Hf_{1-x}Zr_xO_2$ films, grown between TaN and aluminum electrodes, for nominal Zr doping concentrations of $x = 0$, 0.5, 0.7, and 1. As annealing enables crystallization into the ferroelectric phase in $Hf_{1-x}Zr_xO_2$, we report on the effective thermal conductivity values for both annealed and unannealed films. Furthermore, our use of time-domain thermoreflectance (TDTR) for thermal metrology allows for determination of the volumetric heat capacity of selected $Hf_{1-x}Zr_xO_2$ films when deposited on thermally insulating substrates. Thus, we also report on the measured volumetric heat capacity of films for nominal Zr concentrations of $x = 0.5$ and $x = 0.7$, a thermophysical parameter that is critical for further development of devices based on this material, for example, devices leveraging pyroelectric effects.[17,18]

Samples were fabricated by rf-magnetron sputtering a 10 nm thick TaN layer onto (001) silicon substrates. Thermal atomic layer deposition (ALD) was then used to deposit 20 nm thick films of $Hf_{1-x}Zr_xO_2$ for compositions ranging from $0 \leq x \leq 1$. The precursors for the HfO_2 and ZrO_2 cycles included Tetrakis(dimethylamino) hafnium (TDMA Hf) and Tetrakis(dimethylamino)zirconium (TDMA Zr), respectively, at 75 °C, with H_2O used as the oxidant for both. For HfO_2 and ZrO_2, the growth per cycle (GPC) was 0.1086 and 0.0968 nm, respectively, measured via ellipsometry. To control the composition of the $Hf_{1-x}Zr_xO_2$ films, the number of cycles for each precursor was adjusted relative to the other. For example, for $x = 0.5$ (5:5 Hf:Zr), 20 "supercycles" of 5 ZrO_2:5 HfO_2 were utilized, and for $x = 0.7$ (3:7 Hf:Zr), 20 "supercycles" of 7 ZrO_2:3 HfO_2 were utilized. This

a)Electronic mail: phopkins@virginia.edu

process yielded films with a nominal thickness of 20 nm with a variance of 0.068–1.72 nm, depending on the composition. Actual film compositions are $Hf_{0.58}Zr_{0.42}O_2$ for the 5:5 Hf:Zr film and $Hf_{0.36}Zr_{0.64}O_2$ for the 3:7 Hf:Zr film, as determined by x-ray photoelectron spectroscopy on identically prepared samples.[11] To facilitate the thermal property analysis, control samples were also fabricated without a $Hf_{1-x}Zr_xO_2$ layer on both Si and SiO_2 substrates. For further details of fabrication processes, we direct readers to a prior study.[11]

Following fabrication, a subset of the samples were subjected to a 30 s anneal at 600 °C using a rapid thermal annealer in a nitrogen atmosphere. To analyze crystallinity, grazing incidence x-ray diffraction (GIXRD) was performed for samples of each composition. An ω angle of 2° was utilized, and measurements were taken over a range of 26°–33° of 2θ. We find that in the unannealed state, the films are amorphous, in agreement with prior findings for unannealed films.[6] As shown in Fig. 1, after annealing, $Hf_{1-x}Zr_xO_2$ films crystallize into either monoclinic or mixed tetragonal/orthorhombic phases depending upon the concentration of zirconia. For films containing primarily hafnia, the $\bar{1}11$ and 111 reflections of the monoclinic phase are readily apparent at 28.4° and 31.6° in 2θ, respectively.[5,6,11,19] For films with zirconia concentrations greater than or equal to 50%, the intensity of the monoclinic phase reflections is reduced, and 011 and 111 reflections associated with a mixture of the orthorhombic/tetragonal phase are intensified, which occur at approximately 30.4° in 2θ.[1,11,19] Film phase fractions were quantified via the ratios of the integrated peak intensities[20] for the monoclinic and tetragonal/orthorhombic phases. Intensities of the pure HfO_2 (monoclinic) and ZrO_2 (tetragonal) reflections and atomic scattering factor differences with composition were used in normalization to account for structural and compositional dependences of peak intensity, respectively. Volumetric phase fractions of 0.08 monoclinic and 0.92 tetragonal/orthorhombic were calculated for the 3:7 Hf:Zr film and 0.59 monoclinic and 0.41 tetragonal/orthorhombic were calculated for the 5:5 Hf:Zr film.

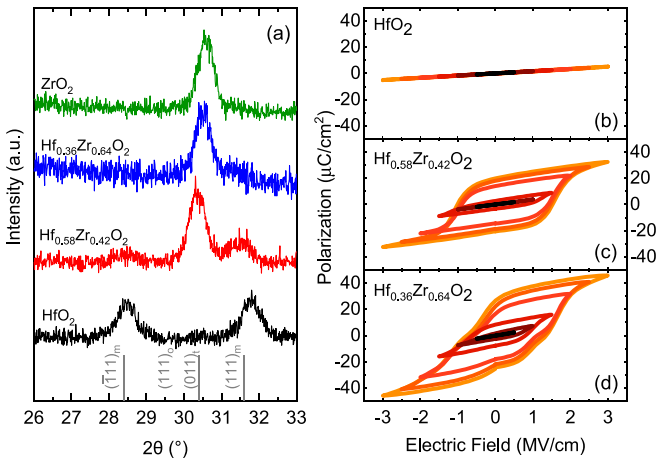

FIG. 1. (a) GIXRD measurements of annealed samples for various compositions of $Hf_{1-x}Zr_xO_2$. (b)–(d) The polarization field responses for the annealed $Hf_{1-x}Zr_xO_2$ films with nominal concentrations of $x = 0$, 0.5, and 0.7, respectively. The black, innermost curves display polarization field responses for an applied voltage of 1 V; the lighter shades, moving outward, display voltage increases in 1 V increments, ending with an applied voltage of 6 V (light orange) for the outermost curve.

To verify ferroelectric responses in the $Hf_{1-x}Zr_xO_2$ films, polarization electric field responses were measured for nominal compositions of $x = 0.5$ and $x = 0.7$ and contrasted against pure hafnia. To make these measurements, contacts were fabricated on the surface of the $Hf_{1-x}Zr_xO_2$ films: a 10 nm electrode layer of TaN was sputtered onto the surface followed by a 70 nm layer of platinum which was rf-magnetron sputtered through a shadow mask in order to create square contacts with side lengths of approximately 635 μm, separated by 2 mm in a two dimensional array. A reactive ion etch was then used to etch the TaN layer in between the platinum contacts leaving isolated electrodes atop the exposed $Hf_{1-x}Zr_xO_2$ layer. Polarization-field measurements were collected with voltage biases ranging from ±1 to ±6 V, as displayed in Figs. 1(b)–1(d). For all as-deposited $Hf_{1-x}Zr_xO_2$ films, we measure a linear dielectric response (not shown). For the annealed HfO_2 sample, as shown in Fig. 1(b), the same linear response can be seen. For annealed samples of $Hf_{0.58}Zr_{0.42}O_2$ and $Hf_{0.36}Zr_{0.64}O_2$, hysteresis is displayed in the polarization-field response, confirming ferroelectric behavior in the films.[8,11]

Following an alcohol clean (five minute sonications in isopropanol, acetone, and methanol, respectively), the samples were then coated with an 80 nm aluminum layer via electron beam evaporation to prepare them for thermal property measurements via time-domain thermoreflectance (TDTR).[21] We utilize a repetition rate of 80 MHz and a central wavelength of 800 nm (bandwidth of 10.5 nm) and spot sizes of 18 and 11 μm in diameter for the pump and probe beams, respectively. The thermal properties of the samples were measured by fitting the ratio of the in-phase to out-of-phase lock-in signals to a thermal model, the particulars of which have been thoroughly detailed in the literature.[21–24]

Due to the thinness of the $Hf_{1-x}Zr_xO_2$ and TaN layers, we do not directly fit for the intrinsic thermal conductivity of the $Hf_{1-x}Zr_xO_2$ layer since we cannot explicitly separate the thermal conductivity of the layer from the interfaces using a single measurement on a single sample.[13,26] Rather, we treat the two layers as an effective resistive interface between the aluminum transducer and the silicon substrate. As such, when modeling the TDTR data, we treat each sample as a two layer system and fit for the effective thermal boundary conductance. In order to quantify the thermal resistance associated with the $Hf_{1-x}Zr_xO_2$ layer (R_{Eff}), we take the inverse of the measured thermal boundary conductance and subtract the thermal resistances measured from the sample without an $Hf_{1-x}Zr_xO_2$ layer (complete calculations are detailed in the supplementary material). The error in the measurement is attributed to measurement repeatability, uncertainty in aluminum thickness, and uncertainty in the interfacial resistance between aluminum and TaN, which has been taken from the literature.[25] For the effective film thermal conductivity, κ_{Eff}, we take the product of the film thickness and the inverse of the thermal resistance. An additional source of uncertainty is introduced here for film thickness variation in the ALD $Hf_{1-x}Zr_xO_2$ films. The results for R_{Eff} and κ_{Eff} are displayed in Figs. 2(a) and 2(b), respectively.

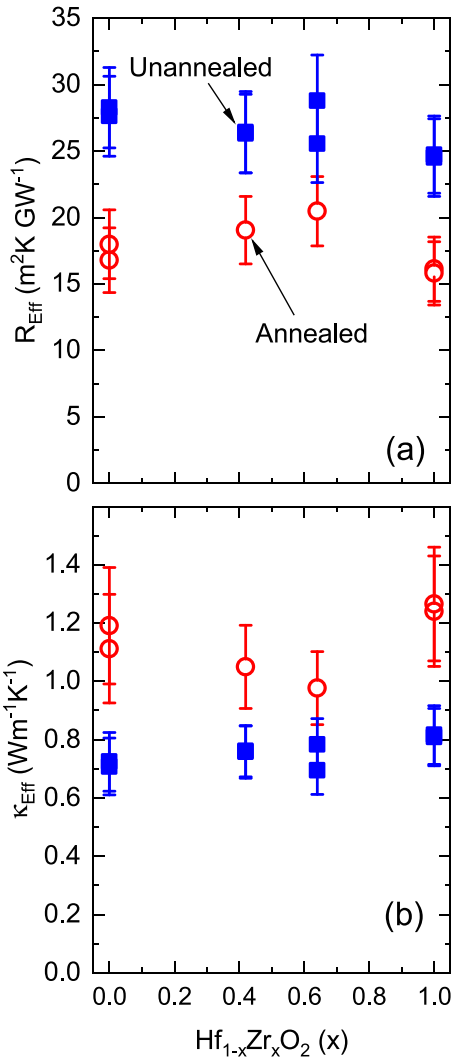

FIG. 2. (a) The effective thermal resistance of the $Hf_{1-x}Zr_xO_2$ films as a function of ZrO_2 concentration, x. (b) recasts this resistance as an effective thermal conductivity, κ_{Eff}, which is the product of the film thickness and the inverse of its associated thermal resistance. In both panels, the unannealed samples are represented by solid blue squares, whereas the annealed samples are represented by open red circles.

In addition to thermal resistance, heat capacity is also of interest for thin $Hf_{1-x}Zr_xO_2$ systems. For nominal compositions of $x = 0.5$ and $x = 0.7$, a second set of samples were fabricated and annealed in the same manner as previously described, on top of a 400 nm layer of SiO_2 on silicon in order to increase sensitivity to the volumetric heat capacity of the $Hf_{1-x}Zr_xO_2$ layer (sensitivity analysis in the supplementary material). To a first approximation, the thermal penetration depth, δ, can be estimated as $\delta = \sqrt{\kappa/(\pi C_v f)}$, where κ is the layer thermal conductivity, C_v is the volumetric heat capacity, and f is the modulation frequency of the pump.[27,28] Setting $\kappa = 1.35\,W\,m^{-1}\,K^{-1}$ and $C_v = 1.65\,MJ\,m^{-3}\,K^{-1}$, the thermal penetration depth in SiO_2 can be estimated as 228 nm for a pump modulation frequency, f, of 5 MHz. More rigorous formalisms provide higher degrees of accuracy for the actual thermal penetration depth;[29–31] however, given that the thickness of the SiO_2 films is 400 nm and all modulation frequencies were above 5 MHz, it is safe to assume that the thermal penetration depth is contained within the SiO_2 layer. As such, we utilize a four-layer model for sensitivity calculations and when fitting for volumetric heat capacity; the four layers consist of an 80 nm aluminum transducer layer, followed by the 20 nm $Hf_{1-x}Zr_xO_2$ films, followed by 10 nm of TaN, on a SiO_2 substrate.

For the four-layer model, we verify the aluminum thickness through profilometry and picosecond ultrasonics[32–35] (80 ± 5 nm), calculate the thermal conductivity via the Wiedemann-Franz law from four-point probe resistivity measurements ($110\,W\,m^{-1}\,K^{-1}$), and assume a literature value of $2.43\,MJ\,m^{-3}\,K^{-1}$ for the volumetric heat capacity at room temperature.[36,37] For the SiO_2 substrate, we apply a thermal conductivity of $1.35\,W\,m^{-1}\,K^{-1}$ and assume a literature value of $1.65\,MJ\,m^{-3}\,K^{-1}$ for the volumetric heat capacity of intrinsic silicon at 300 K.[38] For the TaN layer, we sputter a 10 nm layer of TaN on top of SiO_2 and verify thickness through profilometry (10 ± 1 nm). We measure the effective thermal conductivity in the same manner previously discussed, which is found to be $1.48 \pm 0.21\,W\,m^{-1}\,K^{-1}$. For reference, Bozorg-Grayeli *et al.* have reported values of 3.0 and $3.4\,W\,m^{-1}\,K^{-1}$ as the intrinsic thermal conductivity of TaN films of 50 and 100 nm, respectively.[25] We note that our measured effective thermal resistance of the TaN layer also includes the interfacial resistance between the aluminum transducer and the TaN layer; however, we proceed under the assumption that the resistance attributed to the TaN layer is the dominant resistance. For the lattice heat capacity of TaN, we apply a literature value of $2.94\,MJ\,m^{-3}\,K^{-1}$.[39] Given that the effective thermal conductivities of the $Hf_{1-x}Zr_xO_2$ films were determined from TDTR analyses of the $Al/Hf_{1-x}Zr_xO_2/TaN/Si$ samples, the only unknown of these $Al/Hf_{1-x}Zr_xO_2/TaN/SiO_2$ samples is the volumetric heat capacity of the $Hf_{1-x}Zr_xO_2$ film. To decrease the uncertainty in our reported values of heat capacity of the $Hf_{1-x}Zr_xO_2$ film, we analyze TDTR sensitivity calculations.[40,41] In summary, we find an increase in sensitivity to the heat capacity of the $Hf_{1-x}Zr_xO_2$ layer when there is an SiO_2 layer and also by analyzing the data from the in-phase signal. Therefore, we analyze the in-phase signal for samples of $Hf_{1-x}Zr_xO_2$ concentrations of $x = 0.5$ and $x = 0.7$, fitting only for the heat capacity of that layer. To enhance accuracy further, we analyze data for pump frequencies of 5.82, 8.4, and 12.2 MHz. Further details of the sensitivity analysis can be found within the supplementary material.

A few observable trends in the effective thermal conductivity and thermal resistance of the $Hf_{1-x}Zr_xO_2$ films emerge from Fig. 2. First, it is of note that the effective thermal conductivity is, in most cases, significantly higher when subjected to a 30 s anneal at 600 °C. We attribute this increase to an increase in crystallinity of the film, which was verified through GIXRD. A second, more subtle result, for the annealed samples, shown in Fig. 2, is a slight decrease in the mean effective thermal conductivity for alloys of HfO_2 and ZrO_2. While all effective thermal conductivity values are within error, no definitive claims can be made regarding trends in the data; however, it can be observed that the nominal effective thermal conductivity ranges from 5.8% to 25.7% higher for pure HfO_2 or ZrO_2 compared to alloys of the two. Similar results have been shown in a number of other alloyed material systems owing to alloy scattering of phonons.[47–50] There are no signs of

this trend for the unannealed samples. As the unannealed samples are amorphous and because the measured effective thermal conductivities of the pure hafnia and zirconia films are nearly identical, compositions of the two would yield a negligible change in thermal conductivity. We re-emphasize, however, that these observations are based upon the nominal values of the measurements, and overall trends within the two different datasets (as-deposited and annealed) cannot be concluded with high certainty due to the relatively large uncertainties in these effective thermal conductivities. However, our results do conclusively show that annealing the $Hf_{1-x}Zr_xO_2$ films increases the thermal conductivity, which we attribute to crystallization of the as-deposited amorphous film.

For the results of the heat capacity measurements in Table I, we note that, with their associated uncertainties, the measurements are within error of previously reported measurements for the heat capacity of pure hafnia or pure zirconia. For $Hf_{0.58}Zr_{0.42}O_2$, we report a volumetric heat capacity of 2.18 ± 0.56 MJ m^{-3} K^{-1}, which is slightly lower than prior measurements of pure HfO_2, and 2.64 ± 0.53 for $Hf_{0.36}Zr_{0.64}O_2$. Of the existing measurements for the room-temperature heat capacity measurements of HfO_2, all are of the monoclinic phase.[12,42–44] Because compositions of $x \geq 0.5$ for $Hf_{1-x}Zr_xO_2$ have been shown to also include tetragonal and orthorhombic crystalline phases,[1,11] it could serve to explain why we measure a slightly lower heat capacity. We also note relatively large error bars in our measurement of approximately 30% for the two measurements. While all the fits for the heat capacity have a low mean square error [as can be seen in Fig. 3(a)], we gain further insight into the accuracy of the TDTR data fit for heat capacity by generating a contour in Fig. 3(b), which illustrates uncertainty in the interplay between the effective thermal conductivity and heat capacity of a $Hf_{1-x}Zr_xO_2$ film. We utilize a similar uncertainty contour calculation as has been previously outlined in the literature,[51–54] which calculates the sum of the standard deviation between the fitted thermal model and the measured data, according to the following equation:[52]

$$\sigma = \frac{1}{n}\sum_{i=1}^{n}\left(\frac{X_{m,i} - X_{d,i}}{X_{d,i}}\right)^2, \tag{1}$$

where $X_{m,i}$ and $X_{d,i}$ represent the in-phase values from the thermal model and the measured TDTR data, respectively, at time delay, i, and n is the total number of time delays in a particular TDTR scan. The best fit of the thermal model to the TDTR data provides the lowest value of σ, which we denote as σ_{min}. Therefore, a contour with a constant value of $2\sigma_{min}$ would correspond to a 95% confidence interval for combinations of thermal conductivity and heat capacity which produce a standard deviation less than or equal to $2\sigma_{min}$. As an example, we use Eq. (1) to calculate a σ contour plot for a $Hf_{0.36}Zr_{0.64}O_2$ sample measured with TDTR at a modulation frequency of 8.4 MHz [shown in Fig. 3(b)]. The best fit to the data in this example provides a σ_{min} of 5.05×10^{-5}, and therefore, a 95% confidence interval can be generated by outlining a contour of σ values equal to 1.1×10^{-4}. Therefore, for a given thermal conductivity of 1 W m^{-1} K^{-1}, heat capacity values ranging from 2.1 to 2.5 MJ m^{-3} K^{-1} could be obtained within a 95% confidence interval. As the thermal conductivity of the $Hf_{1-x}Zr_xO_2$ layer is not the only parameter with uncertainty in the thermal model, we utilize propagation of error to take into account uncertainty in the thickness of all films in the stack (Al, $Hf_{1-x}Zr_xO_2$, and TaN), as well as uncertainty in the $Hf_{1-x}Zr_xO_2$ and TaN effective thermal conductivity to obtain the error displayed in Table I.

TABLE I. Room temperature volumetric heat capacities for $Hf_{1-x}Zr_xO_2$. For reference, specific heat values are also provided for $x = 0$ and $x = 1$ and are displayed as volumetric capacities assuming the materials are fully dense.

$Hf_{1-x}Zr_xO_2$ (x)	C_v (MJ m^{-3} K^{-1})	References
0	2.63–2.77	12 and 42–44
0.5	2.18 ± 0.56	This study
0.7	2.64 ± 0.53	This study
1	2.56–2.60	42, 43, 45, and 46

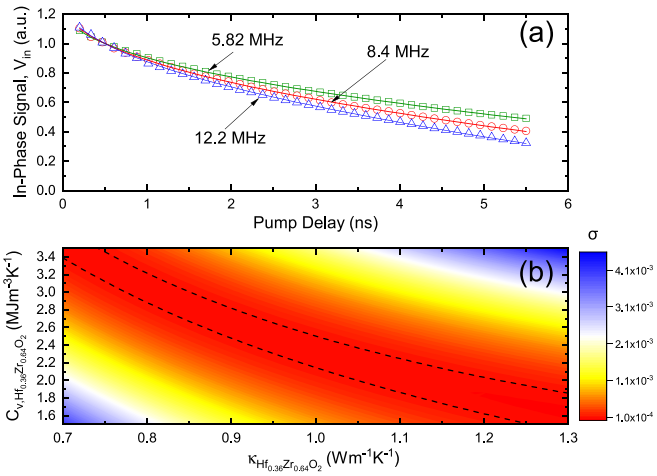

FIG. 3. (a) Representative TDTR data which have been fit for the heat capacity of the $Hf_{0.36}Zr_{0.64}O_2$ film at frequencies of 5.82, 8.4, and 12.2 MHz. The open symbols display measured data, and the solid lines represent their associated fits. (b) A contour plot which displays the standard deviation, σ, between the thermal model and measured TDTR data for the $Hf_{0.36}Zr_{0.64}O_2$ sample at a modulation frequency of 8.4 MHz. The black dashed contour provides a boundary outlining a 95% confidence interval, defined as $2\sigma_{min}$, for a given thermal conductivity.

In summary, we report on the effective thermal resistance of thin films of $Hf_{1-x}Zr_xO_2$ for compositions ranging from $0 \leq x \leq 1$, in addition to the heat capacity of two different film compositions. Ultimately, we find the effective conductivity of the films to be the highest for pure concentrations (in this case, hafnia and zirconia) and slightly decreased for alloys of the two. Furthermore, we note an increased thermal conductivity when films are subjected to a 30 s anneal at 600 °C, which is attributed to the formation of the monoclinic crystalline phase for films consisting primarily of hafnia and tetragonal/orthorhombic crystalline phases for samples alloyed with zirconia. Given the limited nature of literature regarding the thermodynamic properties of hafnia-zirconia systems, and the promise that $Hf_{1-x}Zr_xO_2$ has demonstrated as a ferroelectric material, characterization of its thermal properties in

thin film form is critical for considerations in computing and pyroelectric applications.

See supplementary material for details of the thermal resistance calculations, tabulated data for the thermal measurements, and sensitivity analyses.

Sandia National Laboratories is a multi-mission laboratory managed and operated by National Technology and Engineering Solutions of Sandia, LLC., a wholly owned subsidiary of Honeywell International, Inc., for the U.S. DOE's National Nuclear Security Administration under Contract No. DE-NA-0003525. The views expressed in the article do not necessarily represent the views of the U.S. DOE or the United States Government. This material is based upon work supported by the Air Force Office of Scientific Research under Award No. FA9550-18-1-0352.

[1]P. D. Lomenzo, C.-C. Chung, C. Zhou, J. L. Jones, and T. Nishida, Appl. Phys. Lett. **110**, 232904 (2017).
[2]C. H. Cheng and A. Chin, IEEE Electron Device Lett. **35**, 274 (2014).
[3]M. H. Park, H. J. Kim, Y. J. Kim, T. Moon, K. D. Kim, and C. S. Hwang, Nano Energy **12**, 131 (2015).
[4]S. Mueller, S. R. Summerfelt, J. Muller, U. Schroeder, and T. Mikolajick, IEEE Electron Device Lett. **33**, 1300 (2012).
[5]T. S. Böscke, J. Müller, D. Bräuhaus, U. Schröder, and U. Böttger, Appl. Phys. Lett. **99**, 102903 (2011).
[6]M. Hyuk Park, H. Joon Kim, Y. Jin Kim, W. Lee, T. Moon, and C. Seong Hwang, Appl. Phys. Lett. **102**, 242905 (2013).
[7]X. Sang, E. D. Grimley, T. Schenk, U. Schroeder, and J. M. Lebeau, Appl. Phys. Lett. **106**, 162905 (2015).
[8]J. Müller, T. S. Böscke, U. Schröder, S. Mueller, D. Bräuhaus, U. Böttger, L. Frey, and T. Mikolajick, Nano Lett. **12**, 4318 (2012).
[9]T. Shiraishi, K. Katayama, T. Yokouchi, T. Shimizu, T. Oikawa, O. Sakata, H. Uchida, Y. Imai, T. Kiguchi, T. J. Konno, and H. Funakubo, Appl. Phys. Lett. **108**, 262904 (2016).
[10]S. E. Reyes-Lillo, K. F. Garrity, and K. M. Rabe, Phys. Rev. B-Condens. Matter Mater. Phys. **90**, 140103(R) (2014).
[11]S. W. Smith, A. R. Kitahara, M. A. Rodriguez, M. D. Henry, M. T. Brumbach, and J. F. Ihlefeld, Appl. Phys. Lett. **110**, 072901 (2017).
[12]W. Zhou, Q. Shi, B. F. Woodfield, and A. Navrotsky, J. Chem. Thermodyn. **43**, 970 (2011).
[13]E. A. Scott, J. T. Gaskins, S. W. King, and P. E. Hopkins, APL Mater. **6**, 058302 (2018).
[14]J. T. Gaskins, P. E. Hopkins, D. R. Merrill, S. R. Bauers, E. Hadland, D. C. Johnson, D. Koh, J. H. Yum, S. Banerjee, B. J. Nordell, M. M. Paquette, A. N. Caruso, W. A. Lanford, P. Henry, L. Ross, H. Li, L. Li, M. French, A. M. Rudolph, and S. W. King, ECS J. Solid State Sci. Technol. **6**, N189 (2017).
[15]N. T. Gabriel and J. J. Talghader, J. Appl. Phys. **110**, 043526 (2011).
[16]M. Panzer, M. Shandalov, J. Rowlette, Y. Oshima, Y. W. Chen, P. McIntyre, and K. Goodson, IEEE Electron Device Lett. **30**, 1269 (2009).
[17]R. W. Whatmore, Rep. Prog. Phys. **49**, 1335 (1986).
[18]P. Muralt, Rep. Prog. Phys. **64**, 1339 (2001).
[19]T. Kiguchi, S. Nakamura, A. Akama, T. Shiraishi, and T. J. Konno, J. Ceram. Soc. Jpn. **124**, 689 (2016).
[20]G. Esteves, K. Ramos, C. M. Fancher, and J. L. Jones, LIPRAS: Line-profile Analysis Software (2017), pp. 1–4.
[21]D. G. Cahill, Rev. Sci. Instrum. **75**, 5119 (2004).
[22]A. Schmidt, "Optical characterization of thermal transport from the nanoscale to the macroscale," Dissertation (Massachusetts Institute of Technology, 2008).
[23]D. G. Cahill, K. E. Goodson, and A. Majumdar, J. Heat Transfer **124**, 223 (2002).
[24]P. E. Hopkins, J. R. Serrano, L. M. Phinney, S. P. Kearney, T. W. Grasser, and C. T. Harris, J. Heat Transfer **132**, 081302 (2010).
[25]E. Bozorg-Grayeli, Z. Li, M. Asheghi, G. Delgado, A. Pokrovsky, M. Panzer, D. Wack, and K. E. Goodson, Appl. Phys. Lett. **99**, 261906 (2011).
[26]J. Liu, J. Zhu, M. Tian, X. Gu, A. Schmidt, and R. Yang, Rev. Sci. Instrum. **84**, 034902 (2013).
[27]Y. K. Koh, S. L. Singer, W. Kim, J. M. O. Zide, H. Lu, D. G. Cahill, A. Majumdar, and A. C. Gossard, J. Appl. Phys. **105**, 054303 (2009).
[28]Y. K. Koh and D. G. Cahill, Phys. Rev. B-Condens. Matter Mater. Phys. **76**, 075207 (2007).
[29]J. L. Braun, C. J. Szwejkowski, A. Giri, and P. E. Hopkins, J. Heat Transfer **140**, 052801 (2018).
[30]J. L. Braun and P. E. Hopkins, J. Appl. Phys. **121**, 175107 (2017).
[31]J. Maassen and M. Lundstrom, J. Appl. Phys. **119**, 095102 (2016).
[32]O. Matsuda, M. C. Larciprete, R. Li Voti, and O. B. Wright, Ultrasonics **56**, 3 (2015).
[33]C. Thomsen, H. T. Grahn, H. J. Maris, and J. Tauc, Phys. Rev. B **34**, 4129 (1986).
[34]D. B. Hondongwa, L. R. Olasov, B. C. Daly, S. W. King, and J. Bielefeld, Thin Solid Films **519**, 7895 (2011).
[35]G. A. Antonelli, B. Perrin, B. C. Daly, and D. G. Cahill, MRS Bull. **31**, 607 (2006).
[36]E. H. Buyco and F. E. Davis, J. Chem. Eng. Data **15**, 518 (1970).
[37]A. Sood, R. Cheaito, T. Bai, H. Kwon, Y. Wang, C. Li, L. Yates, T. Bougher, S. Graham, M. Asheghi, M. Goorsky, and K. E. Goodson, Nano Lett. **18**, 3466 (2018).
[38]P. Flubacher, A. Leadbetter, and J. Morrison, Philos. Mag. **4**, 273 (1959).
[39]J. Bryner, D. M. Profunser, J. Vollmann, E. Mueller, and J. Dual, Ultrasonics **44**, e1269 (2006).
[40]B. C. Gundrum, D. G. Cahill, and R. S. Averback, Phys. Rev. B-Condens. Matter Mater. Phys. **72**, 245426 (2005).
[41]A. J. Schmidt, R. Cheaito, and M. Chiesa, Rev. Sci. Instrum. **80**, 094901 (2009).
[42]A. Benyagoub, Phys. Rev. B-Condens. Matter Mater. Phys. **72**, 094114 (2005).
[43]C. Wang, M. Zinkevich, and F. Aldinger, J. Am. Ceram. Soc. **89**, 3751 (2006).
[44]S. S. Todd, J. Am. Chem. Soc. **75**, 3035 (1953).
[45]Y. Touloukian and E. Buyco, *Thermophysical Properties of Matter-Specific Heat: Nonmetallic Solids*, edited by Y. Touloukian and C. Ho (IFI/Plenum, New York, 1970), Vol. 5.
[46]T. Tojo, T. Atake, T. Mori, and H. Yamamura, J. Chem. Thermodyn. **31**, 831 (1999).
[47]R. Cheaito, J. C. Duda, T. E. Beechem, K. Hattar, J. F. Ihlefeld, D. L. Medlin, M. A. Rodriguez, M. J. Campion, E. S. Piekos, and P. E. Hopkins, Phys. Rev. Lett. **109**, 195901 (2012).
[48]Z. Wang and N. Mingo, Appl. Phys. Lett. **97**, 101903 (2010).
[49]B. Abeles, Phys. Rev. **131**, 1906 (1963).
[50]M. C. Steele and F. D. Rosi, J. Appl. Phys. **29**, 1517 (1958).
[51]J. P. Feser and D. G. Cahill, Rev. Sci. Instrum. **83**, 104901 (2012).
[52]X. Wang, C. D. Liman, N. D. Treat, M. L. Chabinyc, and D. G. Cahill, Phys. Rev. B-Condens. Matter Mater. Phys. **88**, 075310 (2013).
[53]A. Giri, J. P. Niemelä, C. J. Szwejkowski, M. Karppinen, and P. E. Hopkins, Phys. Rev. B **93**, 024201 (2016).
[54]C. M. Rost, J. Braun, K. Ferri, L. Backman, A. Giri, E. J. Opila, J. P. Maria, and P. E. Hopkins, Appl. Phys. Lett. **111**, 151902 (2017).